Hailiang Yu
Haitao Gao
Zhou Li

High-Performance Metallic Composites Fabricated by Advanced Rolling Techniques

Springer

High-Performance Metallic Composites Fabricated by Advanced Rolling Techniques

Hailiang Yu · Haitao Gao · Zhou Li

High-Performance Metallic Composites Fabricated by Advanced Rolling Techniques

Springer

Hailiang Yu
Central South University
Changsha, China

Haitao Gao
Central South University
Changsha, China

Zhou Li
Central South University
Changsha, China

ISBN 978-981-97-4330-8 ISBN 978-981-97-4331-5 (eBook)
https://doi.org/10.1007/978-981-97-4331-5

Contents

About the Authors

Dr. Hailiang Yu is a full professor at Central South University. He has been engaged in advanced nonferrous metals and alloy forming and processing. He has published 230 papers and two monographs. He also contributed to two edited books and two chapters. He is currently a member of the Board of Directors of the Nonferrous Metals Society of China, and the Composites Committee of the Nonferrous Metals Society of China. He serves as a key reader of *Metallurgical and Materials Transactions A*, and the editorial board of *Chinese Journal of Mechanical Engineering*, *Journal of Plastics Engineering*, and *Scientific Reports*, and young expert of *Engineering*.

Dr. Haitao Gao is a lecturer at Central South University specializing in the research fields of metal matrix composites and advanced forming technologies for new energy vehicles. Currently, he is in charge of the projects supported by National Natural Science Foundation and the Hunan Provincial Natural Science Foundation. He has filed more than 10 patent applications and published over 30 high-level SCI journal papers. He has been awarded the Second Prize of the China Nonferrous Metal Industry Science and Technology Award.

Dr. Zhou Li is an Associate Professor at Central South University. His research interests include automotive body new materials and advanced forming technology, new energy pure electric vehicle gearbox design and manufacturing. He has also participated in national projects in Australia as a chief investigator, applied for 10 patents, and published 20 papers in high-level journals. He has won the second prize of China Machinery Industry Science and Technology Award, the third prize of "Double Creation" Competition of the European and American Alumni Association.

Chapter 1
Introduction of Fabrication of Metallic Composites

With the rapid development of science and technology, many new requirements for metallic materials are put forward, such as low density, high strength, high wear resistance and corrosion resistance. Under this situation, the unitary metallic material is difficult to meet the needs of industrial production and metallic laminates come into being, which have attracted much attention because of their unique physical and chemical properties [1]. There are many species of metal laminates [2–5], such as Cu/Al, Mg/Al, Al/steel, Cu/invar, and Al/Ti laminates. They have been widely applied in the fields of automobile, aviation, shipbuilding, electronics and chemical industry, such as heat exchanger for automobile [6], aircraft parts [7], ship hull [8], electronic components [9], grounding wire for petrochemical enterprises [10]. The promotion and application of metal laminates are of great significance to solve the outstanding problems of current energy structure and industrial structure [11].

Currently, the preparation technologies of metallic composites have made great progress, which can be divided as liquid–liquid bonding, solid–liquid bonding and solid–solid bonding according to the physical state of matrix metal, as shown in Fig. 1.1. The typical liquid–liquid bonding method is the core filling continuous casting technique. In the fabrication process of metal laminates, the solidification of matrix metal and formation of bonding interface can be simultaneously carried out, which obviously shortens the production process [12]. Nevertheless, core filling continuous casting technique requires very high control precision on the process variables and exhibits the low yield of finial products [13].

Roll-casting technique is regarded as the representative of solid–liquid bonding of metal laminates [14]. Compared with the core filling continuous casting technique, the obvious advantages of roll-casting technique are high production efficiency and low production costs. Moreover, high interfacial bonding strength can be easily obtained under the dual effect of high temperature and rolling pressure [15]. However, the high temperature of liquid metal from another perspective, also leads to the high energy consumption.

H. Yu et al., *High-Performance Metallic Composites Fabricated by Advanced Rolling Techniques*, https://doi.org/10.1007/978-981-97-4331-5_1

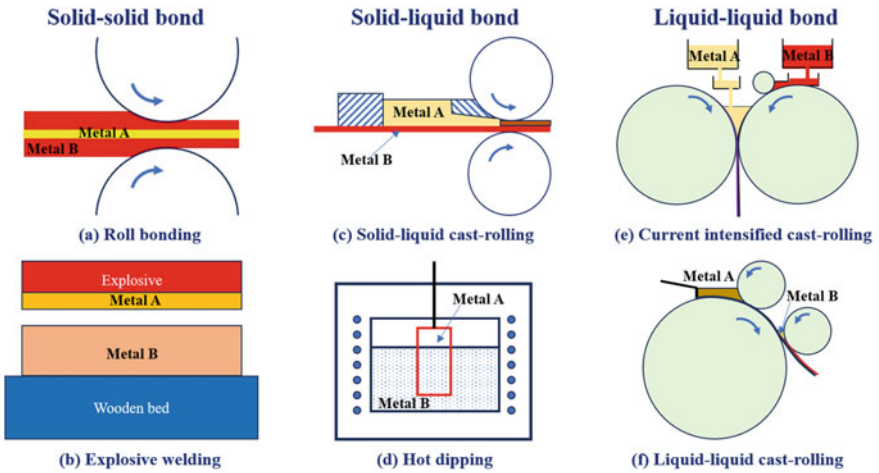

Fig. 1.1 Illustration of techniques for fabrication of metallic composites

Nowadays, the solid–solid method is used for the widest range of industrial application due to its process controllability, which mainly including roll bonding technique [16], extrusion bonding technique [17], and explosive welding technique [18]. Compared with other techniques, the less pollution, stable production process and high production efficiency of roll bonding technique make obvious advantages. In the roll bonding process, the oxidation film on the surface of matrix metal is broken and obvious plastic flow occurs under the action of huge rolling pressure. And then, close contact for these atoms around the bonding interface are carried out. Finally, metallurgical bonding interface can be formed through the heat input and atomic diffusion. Before roll bonding, surface treatment is usually adopted to remove the grease or dirt and expose the fresh matrix metal. Moreover, the annealing process is also necessary to regulate the thickness of intermetallic compound (IMC) layer [19].

In this book, the recent efforts and advances in the roll bonding of metal laminates are summarized to reveal the potential mechanism. Based on the comprehensive understanding and our numerous original works, some important issues about the fabrication method, evolution mechanism of bonding interface and reinforcement factors of roll-bonded metal laminates are introduced.

References

1. Gao HT, Kong C, Yu HL (2023) Lightweight metal laminated plates produced via (hot, cold and cryogenic) roll bonding: a review. Trans Nonfer Met Soc China 33:337–356
2. Khojastehnezhad VM, Pourasl HH (2018) Microstructural characterization and mechanical properties of aluminum 6061–T6 plates welded with copper insert plate (Al/Cu/Al) using friction stir welding. Trans Nonfer Met Soc China 28:415–426

3. Ding YL, Wang JG, Zhao M, Ju DY (2018) Effect of annealing temperature on joints of diffusion bonded Mg/Al alloys. Trans Nonfer Met Soc China 28:251–258
4. Li CL, Fan D, Yu XQ, Huang JK (2019) Residual stress and welding distortion of Al/steel butt joint by arc–assisted laser welding–brazing. Trans Nonfer Met Soc China 29:692–700
5. Nie QQ, Chen GH, Wang B, Yang L, Tang WM (2021) Process optimization, microstructures and mechanical/thermal properties of Cu/Invar bi–metal matrix composites fabricated by spark plasma sintering. Trans Nonfer Met Soc China 31:3050–3062
6. Zu GY, Wang N, Yu JM, Wen JL (2003) Application of composite brazing aluminum foil technology in automotive heat exchanger production. Autom Tech Mater 12:37–38
7. Wang XL, Wei YH (2016) Application and development of metal matrix composites in the aerospace field. Sci Tech Innov Herald 6:16–18
8. Chen YL (1990) New technology of composite materials for shipbuilding. Fiber Reinforced Plastics/Compos 3:17
9. Hartley WD, Garcia D, Yoder JK, Poczatek E, Forsmark JH, Luckey SG, Dillard DA, Yu HZ (2021) Solid–state cladding on thin automotive sheet metals enabled by additive friction stir deposition. J Mater Process Tech 291:117045
10. Liu B (2011) Application of copper–steel composites and exothermic welding technology in the grounding system of petrochemical enterprises. China New Tech Prod 8:14
11. Wang T, Qi YY, Liu JL, Han JC, Ren ZK, Huang QX (2020) Research progress of metal laminates roll bonding process at home and abroad. J Harbin Inst Tech 52(6):42–56
12. Xue ZY, Liang H, Yu WH, Wu CJ (2013) Orthogonal tests of copper–clad aluminum bimetal continuous casting by nitrogen pressure core–filling. China Foundry 10(6):385–390
13. Su YJ, Liu XH, Huang HY, Liu XF, Xie JX (2011) Interfacial microstructure and bonding strength of copper cladding aluminum rods fabricated by horizontal core–filling continuous casting. Metall Mater Trans A 42:4088–4099
14. Liu SY, Wang AQ, Lu SJ, Xie JP (2018) High–performance Cu/Al laminated composites fabricated by horizontal twin–roll casting. Materialwiss Werkstofftech 49:1213–1223
15. Wang ZJ, Li YW, Zhang WN, Wang GD, Liu HT (2021) Microstructural evolution and mechanical properties of titanium–alloying high borated steel sheets fabricated by twin–roll strip casting. Mater Sci Eng A 811:141067
16. Kim IK, Hong SI (2013) Effect of heat treatment on the bending behavior of tri–layered Cu/Al/Cu composite plates. Mater Des 47:590–598
17. Rhee KY, Han WY, Park HJ, Kim SS (2004) Fabrication of aluminum/copper clad composite using hot hydrostatic extrusion process and its material characteristics. Mater Sci Eng A 384:70–76
18. Loureiro A, Mendes R, Ribeiro JB, Leal RM, Galvão I (2016) Effect of explosive mixture on quality of explosive welds of copper to aluminum. Mater Des 95:256–267
19. Yu Y, Song HW, Chen Y, Xu Y, Zhang SH, Wang SD (2014) Investigation on fabrication and mechanical property of ultra–thin Cu/Al clad strip used for coax. Mater Sci Tech 22(5):13–18

Chapter 2
Fabricated Metal Laminates via Hot Roll Bonding Techniques

2.1 Introduction of Hot Roll Bonding Technique

The hot roll bonding technique of metal laminates initially appeared in the 1940s, which is usually applied in the fabrication of thick plate. The hot roll bonding technique can reduce the rolling force but with weak production stability. Before hot roll bonding, matrix metals are preheated to a certain temperature, which will significantly affect the comprehensive properties of metal laminates. Low preheated temperature may lead to the high resistance to deformation and insufficient atomic diffusion around the bonding interface. Nevertheless, the formation of thick IMC layer, even the interfacial cracks, is easily induced by the high preheated temperature. Moreover, protective atmosphere is generally adopted in the hot roll bonding process to avoid the oxidation of interfacial metal [1].

Numerous works about hot roll bonding of metal laminates have been carried out. Menon and Chen [2] used hot roll bonding and annealing to fabricate crack-free laminate s of Al_2O_3 and ZrO_2 with a layer thickness of 4–60 μm. Ag/Cu laminates were fabricated by roll bonding at different temperatures and annealing for different periods at 673 K and 1073 K by Zhang et al. [3]. They found that the speed of Cu atoms moving into the Ag side was faster than that of Ag atoms moving into Cu side. Peng et al. [4] fabricated Cu/Al laminates by hot roll bonding at 703 K with a 60% reduction ratio in a single pass. At lower sintering temperature, $CuAl_2$ appeared at the interface. As the temperature increased, Cu_9Al_4 phase increased. Luo et al. [5] found that the growth rate of IMCs at the bonding interface of the hot-rolled Al/Mg laminate increased with the rising of annealing temperature and the mathematical relationship between the IMCs thickness, annealing temperature and annealing time was built as Eq. (2.1):

$$y^2 = 1.98 \times 10^6 \exp\left(-\frac{83418}{RT}\right)\left(t - 0.78 \exp\frac{29770}{RT}\right) \tag{2.1}$$

H. Yu et al., *High-Performance Metallic Composites Fabricated by Advanced Rolling Techniques*, https://doi.org/10.1007/978-981-97-4331-5_2

where y was the thickness of IMCs layer (μm), T was the annealing temperature (K), R was the Boltzmanns constant (8.314 J/(mol·K)), t was the annealing time (min). Cui et al. [6] thought that roll bonding and subsequent reaction annealing laminates were a feasible near-net-shape processing method for the production of Ti/(TiB_2/Al) laminates.

2.2 Interface Bonding Behavior During Hot Deformation

A series of experiments on interface bonding in a low-carbon steel under hot plastic deformation were carried out using the thermo-mechanical simulator. The main influence factors such as the heating temperature, holding time, reduction ratio, strain rate and number of deformation passes on the interface bonding behavior in the laminates were analyzed using SEM imaging. The results provide sufficient basis for further research on interface bonding and propagating in steel during plastic deformation, and also on quality control in roll bonded products [7].

2.2.1 Interface Bonding Behavior Affected by Heating Temperature

Figure 2.1 gives SEM micrographs of the interface bonding zone for different heating temperatures. There is an obvious commencement of interface bonding when the heating temperature is 1173 K. At this stage, the macro-debonding regions disappear, but there are still many small holes and small grains of size less than 10 μm in the interface zone, and the microstructure is only ferrite compared with that of the overall matrix. When the heating temperature reaches 1273 K, the interface bonding is clearly better, and fewer and smaller holes remain in the transitional zone where the grain size increases and the microstructure is still ferrite. When the heating temperature reaches 1373 K, the holes undergo further reduction in size and the microstructure is similar to the matrix of some pearlite. There are no holes in the entire interface zone, and the microstructure around the interface zone is similar to that of the matrix when the heating temperature reaches 1473 K. The figures show that the degree of interface bonding quality increases progressively and the transitional zone of residual voids gradually disappears with increasing the heating temperatures.

The relationship between the number of residual holes and the heating temperature (T_H) is shown in Fig. 2.2. Curve-fitting yields the following equation:

$$y = 5.04 \times 10^{13} \exp(-T_H/42.16) + 1.23 \tag{2.2}$$

The deformation resistance of the samples decreases as the heating temperature increases. Thus, the protrusions on the interfaces will deform more easily under

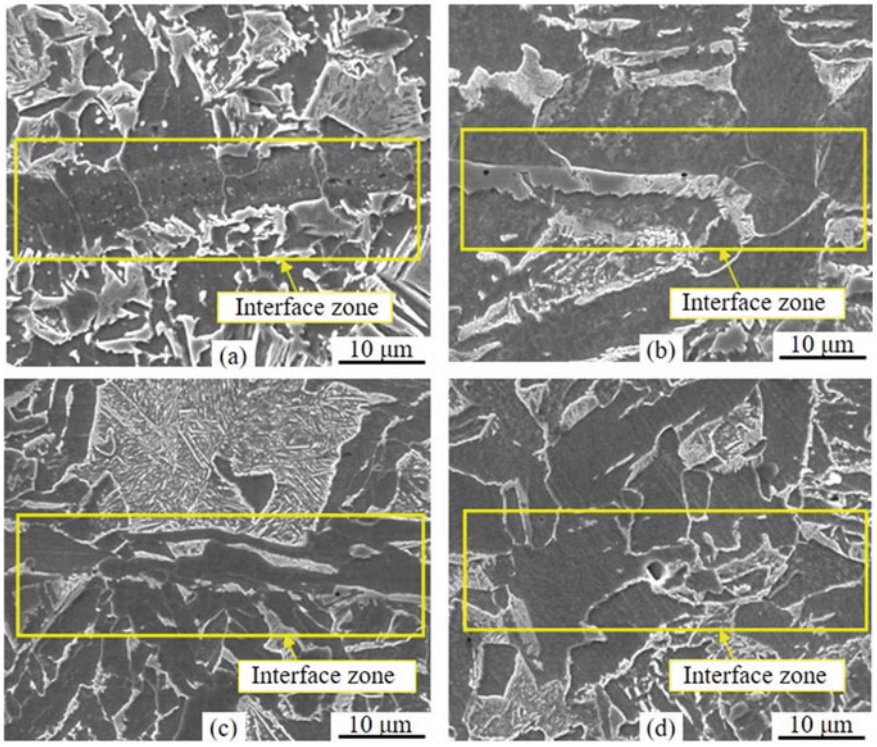

Fig. 2.1 SEM micrographs of interface bonding zone after deformation for various heating temperatures. **a** 1173 K, **b** 1273 K, **c** 1373 K, and **d** 1473 K

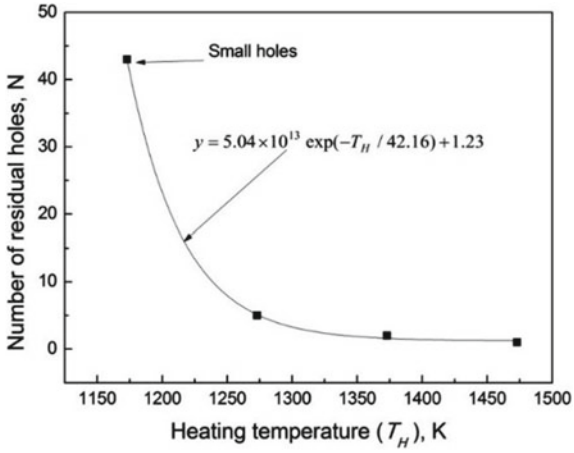

Fig. 2.2 Number of residual holes in the interface bonding zone after deformation as a function of heating temperatures

compression. When the contact surface increases, the density of residual holes around the interface bonding zone decreases. The relationship between the diffusion coefficient and the heating temperature can be calculated by Arrhenius formula,

$$D = D_0 \exp(-Q/RT) \tag{2.3}$$

where D is the diffusion coefficient, D_0 is the diffusion constant, Q is the molar activation energy of diffusion, R is the universal molar gas constant, and T is the thermodynamic temperature.

With increasing the heating temperature, the atoms on the interfaces can migrate more easily, corresponding to the higher diffusion coefficient. This leads to enhanced interface bonding quality. Simultaneously, the higher the heating temperature is, the more easily the grains around the interface zone grow, which accelerates the migration of defects, and results in narrowing the bonding transitional zone.

2.2.2 *Interface Bonding Behavior Affected by Reduction Ratio*

Figure 2.3 shows SEM micrographs of the center of the interface bonding zone of specimens after compressive deformation for various reduction ratios. In Fig. 2.3a, the majority of interface zone is still in a disconnected state when the reduction ratio is zero. Although the reduction ratio is set to zero, a very small reduction occurs in the holding process. The temperature around interfaces is not uniform due to the non-uniform thermal resistance in the interface zone with the current power heating. This induces bonding in parts of the interface zone. Bonding is not seen in the other zones because the normal distance between interfaces is too large and the atoms cannot jump directly across the gap. When the reduction ratio is 10%, the bonding area in the interface zone increases, and most parts of interface zones bond together. However, the degree of interface bonding is not high, and a number of large holes can be seen in the interface zone, as shown in Fig. 2.3b. During the compressive deforming, the protrusions on the interfaces come into contact first, which enlarge the contact surface in the bonding zone, so that the interfaces bond due to a combination of atomic diffusion under the stress and thermal gradients. The interfaces do not come into full contact for this reduction ratio, leaving some residual holes. SEM micrographs of the interface bonding zone shown in Fig. 2.3c and d correspond to an increased reduction ratio of 20% and 30% respectively. Here, the hole size decreases significantly compared to that in Fig. 2.3b. It is also seen from Fig. 2.3a–d that the microstructure in the interface bonding transitional zone consists of only ferrite [8]. When the reduction ratio is 40%, it is difficult to detect holes remaining in the interface zone after deformation. But there is still an obvious transitional zone whose microstructure is different from that of the overall matrix. The grain size in the bonding transitional zone is smaller than that of the matrix,

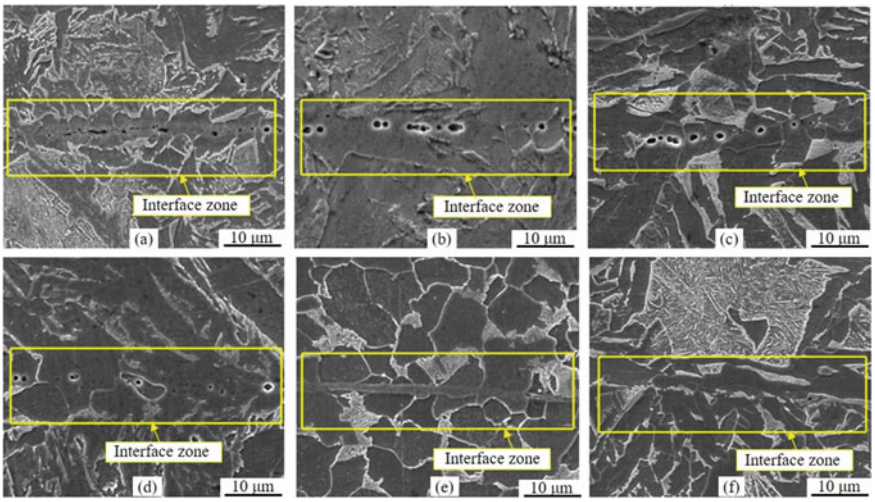

Fig. 2.3 SEM micrographs of interface bonding zone for different reduction ratios. **a** 0%, **b** 10%, **c** 20%, **d** 30%, **e** 40% and **f** 50%

as shown in Fig. 2.3e. When the reduction ratio increases to 50%, the grains in the interface bonding zone are similar to those in the matrix, whose microstructure is no longer only ferrite, as shown in Fig. 2.3f.

Figure 2.4 shows the relationship between the number of residual holes in the interface bonding zone and reduction ratio (R), which is fitted well by Eq. (2.4).

$$y = 23.07 - 0.88R + 0.01R^2 \tag{2.4}$$

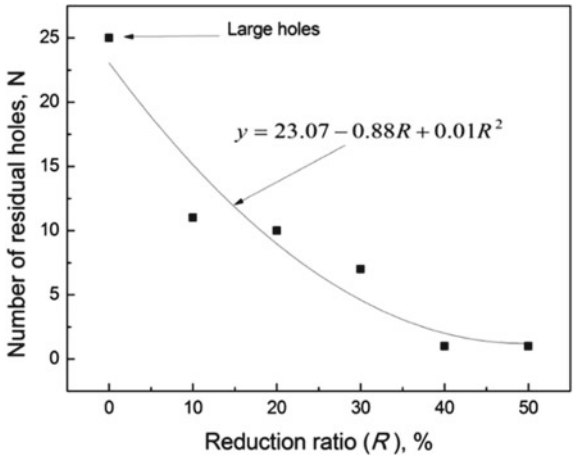

Fig. 2.4 Number of residual holes in the interface bonding zone after deformation as a function of reduction ratios

It is seen that as the reduction ratio increases, the interface bonding degree in the interface zone increases, the interface bonding transitional zone gradually narrows, and the difference in the microstructure between the transitional zone and the matrix also reduces. With greater reduction ratio, the deformation of the protrusions on the interfaces increases, increasing the contact surface. For a given deformation temperature, the diffusion driving force caused by the temperature is unchanged. With increasing deformation, the stress gradient increases, so that the diffusion driving force for atomic diffusion on the interfaces increases. This accelerates the formation of bonds across the interfaces. At the same time, as the reduction ratio increases, the driving force of atomic diffusion also increases, increasing the energy of the lattice distortion.

2.2.3 Interface Bonding Behavior Affected by Deformation Pass Number

Figure 2.5 shows SEM micrographs of the interface bonding zone after compressive deformation for different number of deformation passes, with the total reduction ratio held constant value of 50%. There are some residual small holes in the interface bonding transitional zone after the fifth deformation pass with 10% reduction per pass. When the number of deformation passes is three (reduction schedule 20 + 20 + 10%), there are still small holes in the interface bonding transitional zone, and the microstructure in the interface bonding transitional zone becomes more uniform in the matrix. When the schedule of the deformation is 30 + 20% (two passes), the holes decrease further in size/number. When the reduction ratio is 50% in one pass, there are very few holes which remain in the interface zone after deformation.

It is seen that the number of residual holes in the interface zone after deformation decreases as the number of deformation pass decreases when the total reduction ratio is constant, so that the interface bonding degree improves. The relationship between the number of residual holes and the number of deformation pass is approximate linear relationship, as shown in Fig. 2.6. For the same total reduction ratio, the deformation in every pass can be specified; as the number of the deformation pass increases, the deformation in every pass decreases. Due to the short-range Van der Waals forces, the deformation in every pass will just occur at the sample surface when the number of deformation pass is large enough. The total deformation reaches the set reduction ratio after multi-pass deformation, and the deformation at the center of sample will be still small, which will result in lots of residual holes in the interface zone, thus the interface bonding degree decreases.

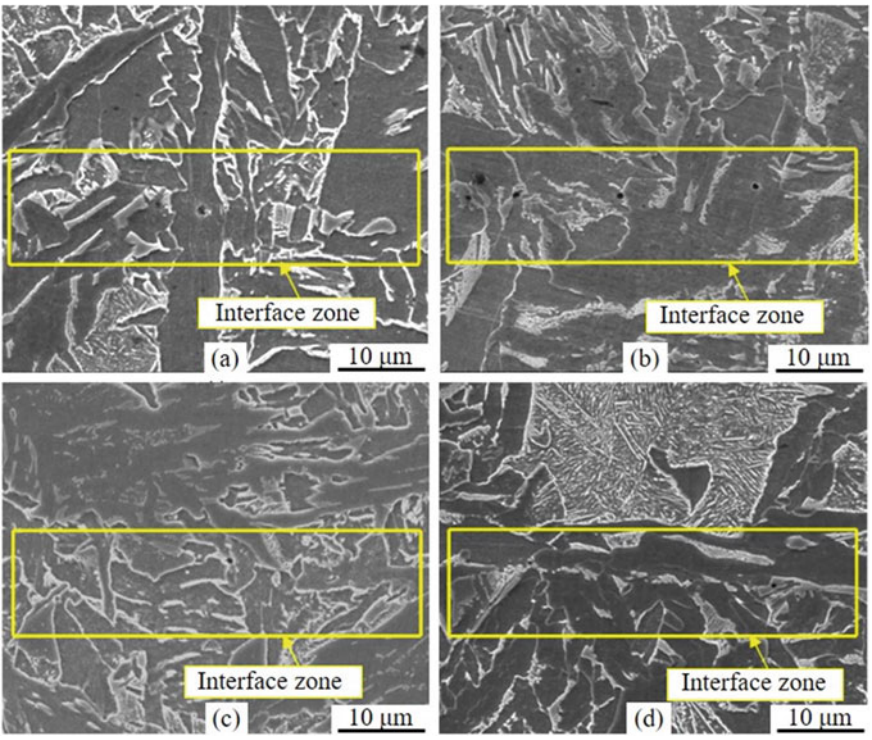

Fig. 2.5 SEM micrographs of interface bonding zone for various deformation passes with identical total reduction ratio. **a** Five passes, **b** Three passes, **c** Two passes, and **d** One pass

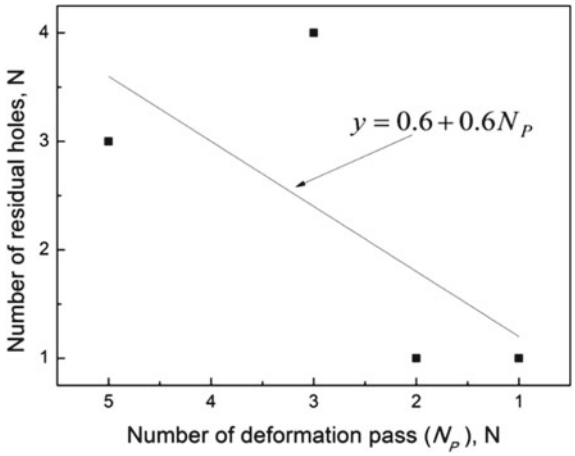

Fig. 2.6 Number of residual holes in the interface bonding zone after deformation as a function of number of deformation passes with the same total reduction ratio constant value

2.2.4 Interface Bonding Behavior Affected by Strain Rate

Figure 2.7 shows SEM micrographs of the interface bonding zone after compressive deformation at various strain rates. When the strain rate is 15 s^{-1}, there are holes which are distributed linearly at the interface zone and the size of holes is large. When the strain rate is 5 s^{-1}, the number of small holes decreases, and interface bonding improves. When the strain rate is 1 s^{-1}, the interface bonding degree in the interface zone improves further. It is difficult to detect the holes visually in Fig. 2.7c. When the strain rate is 0.01 s^{-1}, the interface bonding degree is the highest, and the transitional zone cannot be visually identified.

The relationship between the number of residual holes and the strain rate is shown in Fig. 2.8. With decreasing in the strain rate, the number of residual holes in the interface zone obviously decreases, and the interface bonding quality increases. The atomic diffusion coefficient on the interfaces and recrystallization around the interface zone are affected by the strain rate. Elimination of the gap between interfaces is affected by recrystallization in the interface zone. Firstly, the nucleus deforms, and then the grain grows. With increasing in grain size, the necessary material is moved

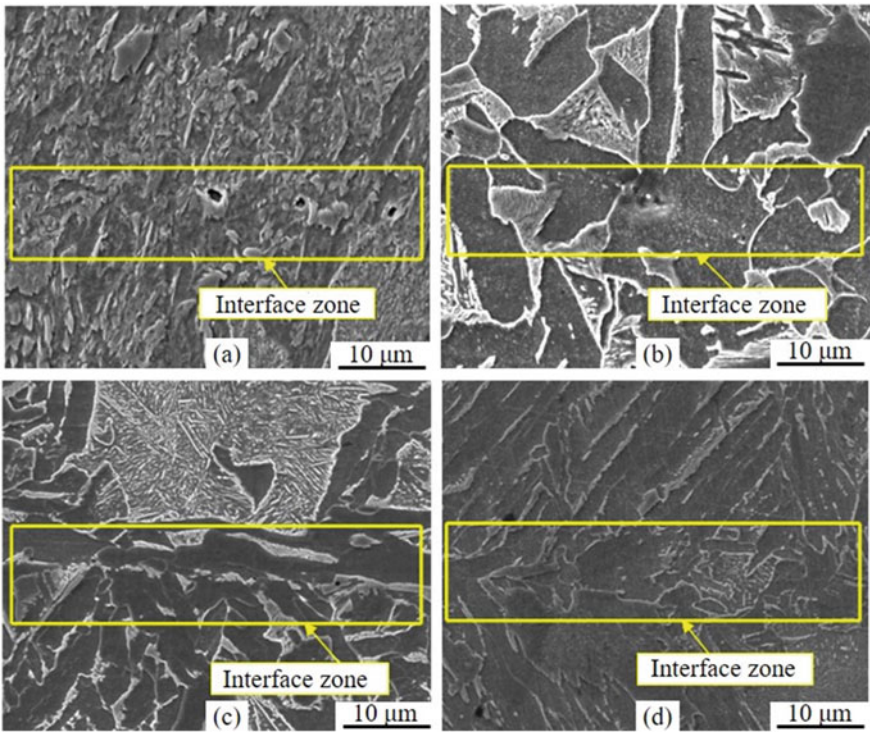

Fig. 2.7 SEM micrographs of interface bonding for various strain rates. **a** 15 s^{-1}, **b** 5 s^{-1}, **c** 1 s^{-1}, and **d** 0.01 s^{-1}

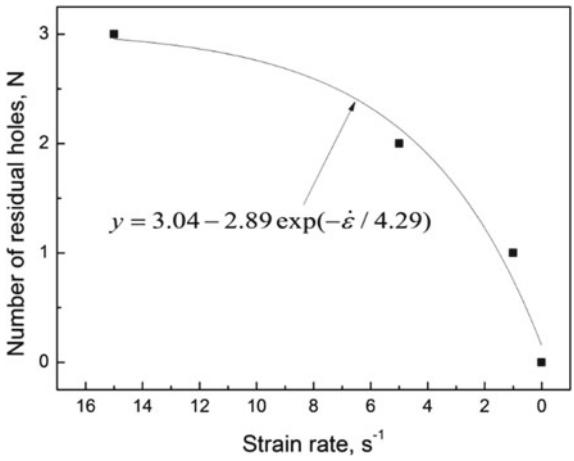

Fig. 2.8 Number of residual holes in the interface bonding zone after deformation as a function of strain rates

by diffusion from the matrix. So, a new weak zone might emerge near the interface. If the recrystallization occurs rapidly, and the atoms far away from the interfaces cannot diffuse immediately. So, some holes will remain in the interface zone. As the strain rate increases, the holes increase in size/number and the interface bonding quality decreases. In addition, with increasing strain rate, the holding time for interface bonding will decrease. As seen in the following section, the holding time is one of the main factors influencing interface bonding quality. The shorter the holding time, the less adequate is the atomic diffusion. The average distance between atoms is directly proportional to the square root of diffusion time, as shown in Eq. (2.5):

$$X = K\sqrt{\tau} \tag{2.5}$$

where X is the average migration distance of the atomic diffusion (mm); τ is the diffusion time (s); K is the constant related to material (mm·s$^{-1/2}$).

2.2.5 Interface Bonding Behavior Affected by Holding Time

Figure 2.9 shows SEM micrographs of the interface bonding zone after compressive deformation for different holding time durations. When the holding time is 1 min, some residual holes linearly distribute in the interface zone. When the holding time is 5 min, there are new grains formed in the interface zone, but there still is an obvious transitional zone of interface bonding. When the holding time is 10 min, the transitional zone becomes unclear, and the size of the holes decreases. When the holding time reaches 20 min, the grain size in the interface zone is similar to that of the matrix, and the interface bonds quite well. These results show that the interface bonding quality improves with extension of the holding time.

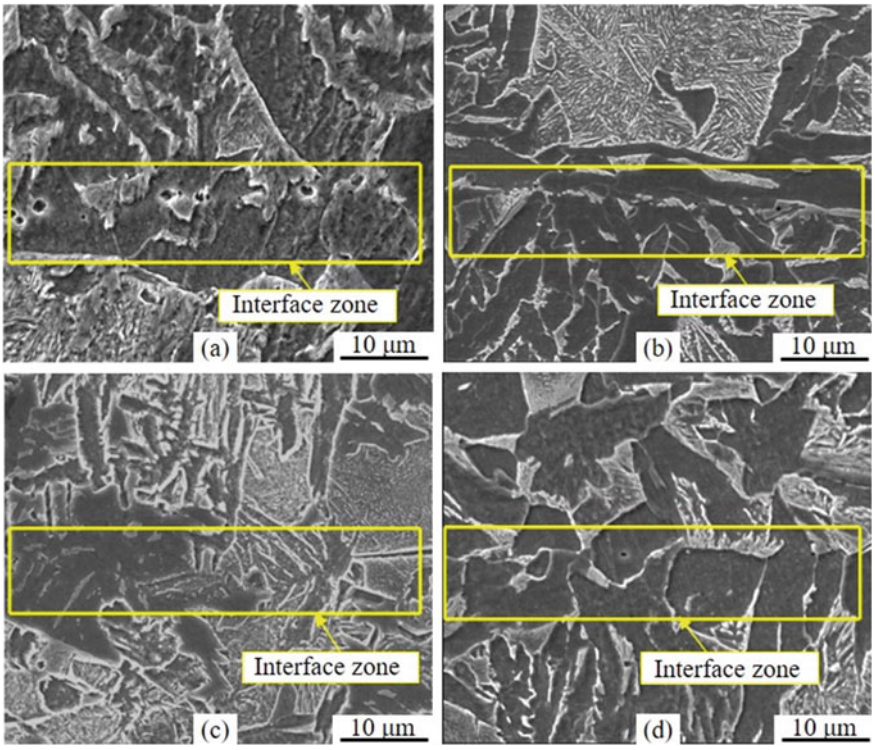

Fig. 2.9 SEM micrographs of interface bonding zone for various holding time durations. **a** 1 min, **b** 5 min, **c** 10 min, and **d** 20 min

Figure 2.10 shows the relationship between the number of residual holes and the holding time. With longer holding time durations, the number of residual holes reduces greatly.

With extension of holding time, there is sufficient opportunity for atomic diffusion to occur around the interface zone, contributing to interface bonding, and uniformity in the microstructure. According to the Fick's second law of diffusion,

$$\frac{\partial C}{\partial t} = D\frac{\partial^2 C}{\partial x^2} \tag{2.6}$$

where, the atomic concentration C is a function of the diffusion distance x and the diffusion time t. The diffusion distance is directly proportional to the square root of the diffusion time, as shown in Eq. (2.6). The holding time plays a key role at the beginning of bonding processes, and its effect gradually decreases with extension of the holding time. As far as its contribution to atomic diffusion is concerned, the effect of holding time is just less than that of heating temperature. The heating time

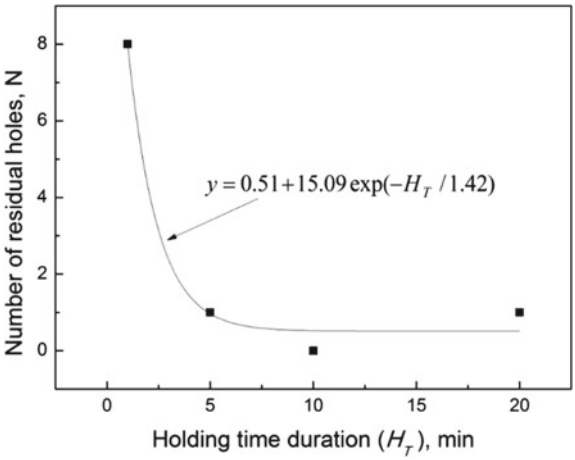

Fig. 2.10 Number of residual holes in the interface bonding zone after deformation as a function of holding time durations

impacts the bonding quality at the beginning and the interfaces can bond completely when the heating time is long enough.

2.3 Shear Strength of Hot-Rolled Laminates

According to the designed shape shown in Fig. 2.11, the samples are machined through the wire-cut machine, which are used for measuring the bonding strength by using the tensile testing machine [9].

Figure 2.12 shows the fracture form of the samples. For the samples subjected to 5% reduction ratio, the sample fractures along the bonding interface, as shown in Fig. 2.12a; for the samples subjected to the 50% reduction ratio (Fig. 2.12b), the sample fractures along the sample matrix, which means that the strength of bonding zone approximately equals that of the matrix and the bonding is quite well.

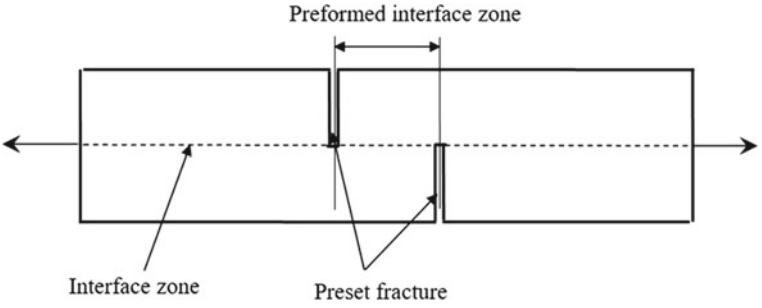

Fig. 2.11 Schematic drawing of tensile sample for measuring bonding strength

Fig. 2.12 Tensile fracture of roll bonded samples

Figure 2.13 shows the curve of load versus displacement during stretching. When the reduction ratio is 5%, the maximum extension of length is 1 mm, and the maximum tension is 100 MPa. When the reduction ratio reaches 50%, the maximum extension of length is 5 mm, and the maximum tension reaches 240 MPa. In order to compare the effects of rolling reduction ratio on bonding quality, the maximum shear strength is employed in the following, which equals the maximum tension versus the area of preformed bonding zone.

Figure 2.14 shows the shear strength of the preset bonding zone after hot rolling under a variety of reduction ratios. When the reduction ratio is less than 10%, the shear strength of bonding zone linearly increases from 0 to 160 MPa with increasing the rolling reduction ratios. As the reduction ratio further increases, the shear strength of the bonding zone also gradually increases, but the amplification gradually decreases. When the reduction ratio reaches 40%, the shear strength of bonding zone reaches 200 MPa. In Fig. 2.14, when the reduction ratio is 50%, the samples break along

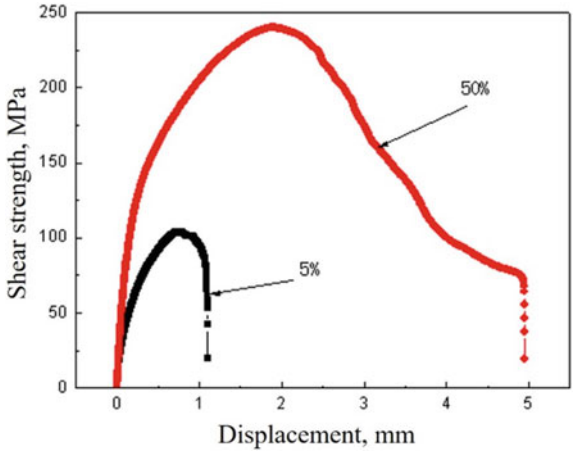

Fig. 2.13 Curve of load to dislocation during stretching

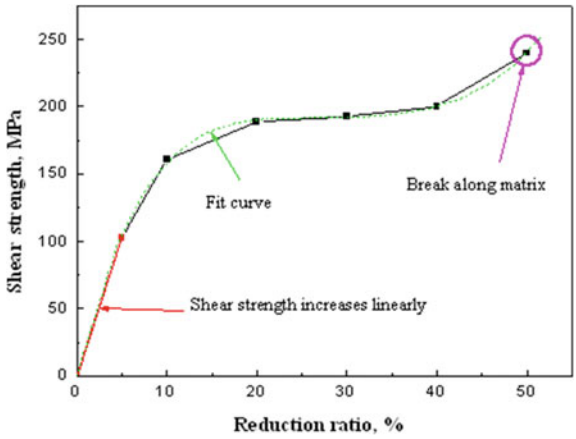

Fig. 2.14 Shear strength of bonding zones for various reduction ratios

the matrix and the tensional stress reaches 240 MPa, the strength of slab matrix. Equation (2.7) can be used to calculate the shear strength of bonding surface under a variety of reduction ratios during rolling.

$$\sigma_T = -0.45179 + 28.01148\varepsilon - 1.60209\,\varepsilon^2 + 0.04544\varepsilon^3 - 6.55158 \times 10^{-4}\,\varepsilon^4 + 4.0331 \times 10^{-6}\varepsilon^5 \quad (2.7)$$

where, σ_T is the shear strength, ε is the reduction ratio.

Figure 2.15 shows the fracture morphology of bonding zones under various reduction ratios during hot roll bonding, where the reduction ratio in (a)–(f) is 5%, 10%, 20%, 30%, 40% and 50% separately. When the reduction ratio is 5%, in the whole view of fracture surface, a small number of zones are dimple fracture which means that these zones can achieve good bonding, but most zones are cleavage fracture where the interface does not bond well (Fig. 2.15a). When the reduction ratio is 10%, the dimple fracture zone increases clearly (Fig. 2.15b) and this means that the bonding quality increases. When the reduction ratio reaches 20–30%, as the reduction ratio further increases, the size and the number of dimple fracture zones increase greatly (Fig. 2.15c and d). However, the dimple fracture zones do not connect with each other. When the reduction ratio is 40%, the fracture type of samples is completely dimpling fracture (Fig. 2.15e), which implies the interface bonding excellent, which is similar to that in Fig. 2.15f, which fractures along the sample matrix.

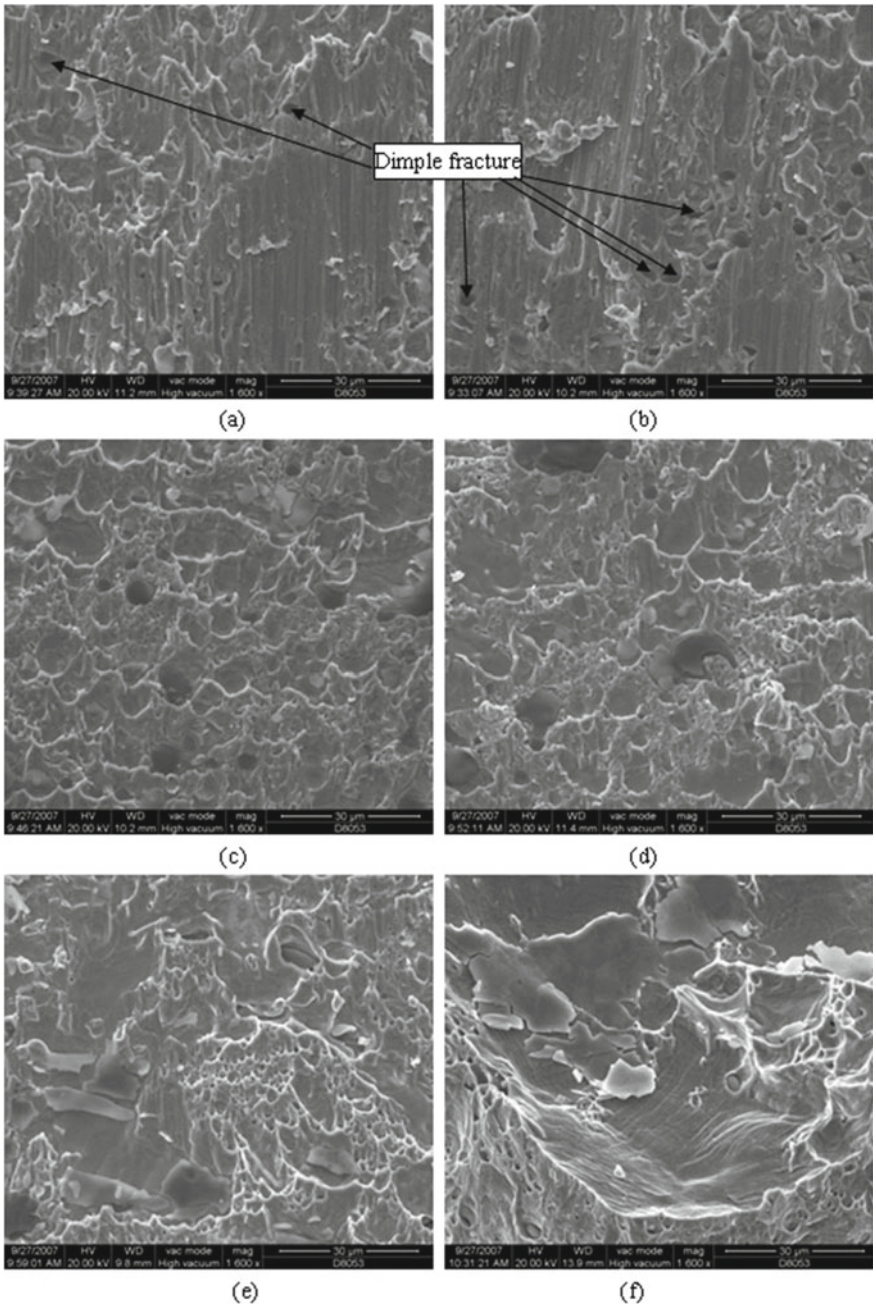

Fig. 2.15 Fracture morphology of bonding zones under the reduction ratio of **a** 5%, **b** 10%, **c** 20%, **d** 30%, **e** 40%, and **f** 50% during hot roll bonding

2.4 Interface Bonding Mechanism of Laminates During Hot Roll Bonding

The recrystallization in the ferrite and the grain growth during the process of interface bonding are shown schematically in Fig. 2.16 [10]. In the process of hot roll bonding, high temperature combined with severe plastic deformation can induce interface bonding. At high temperature, recrystallization can occur at the free interfaces, as shown in Fig. 2.16a. With increasing the energy input by severe plastic deformation, an uneven distribution of energy on the interface can lead to different deformation intensity on the interfaces. Tiny grains will appear and grow towards the gap, resulting in shrinking the gap gradually, shown in Fig. 2.16b. Usually, surfaces in materials are uneven and the convex surfaces come into contact firstly. In other words, interface bonding is initiated at such points of contact. The interfaces can only be partially joined or welded to reach the threshold of atomic interactions under the rolling pressure, the remaining regions can be bonded through the atomic movement, as shown in Fig. 2.16c. Thus, the original long interface is divided into several discontinuous shorter holes. When the atoms on both sides of interfaces come within the range of atomic interactions, intermittent partial interface bonding will take place, and the interface bonding area appears as a distribution of porosity defects, as shown in Fig. 2.16d. The existence of interface can increase the system energy, leaving the system in an unstable state. However, new grain nucleation and growth can utilize this excess energy. New grains will form around these gaps. The new grains nucleate and grow or near the defect free surface during slow cooling which can be called the repair recrystallization, and then the bonding area extends. Tiny grains, which appear in local bonding areas, whose growth regions will continue to grow until their sizes are close to matrix grains, shown in Fig. 2.16e.

2.5 Cu/Al Laminates with Thin SUS304 Interlayer via Hot Roll Bonding

Cu/Al/Cu laminates with thin SUS304 interlayer of 30 μm were fabricated by hot roll bonding. The T2 Cu and AA1060 sheets were used as start materials. The Cu and Al sheets were annealed at 873 K and 673 K for 2 h respectively to obtain a fully homogeneous coarse grain structure, and then cut into a same size of 100 × 50 × 1 mm. Before roll bonding, the Cu and Al sheets were wire brushed to remove the surface oxide layer and contamination. Then the Cu, Al and SUS304 sheets were stacked together and fixed by aluminum rivets. The stacked sheets were preheated at 723 K for 1 min and then rolled at a speed of 1 m/min. Table 2.1 illustrates roll bonded Cu/Al/Cu clad sheets under different condition.

The ordinary laminate rolling bonding is an effective and efficient process to manufact large volume laminates continuously, which also avoid the additional welding process. In this study, the SUS304 interlayer was introduced in Cu/Al/Cu laminates

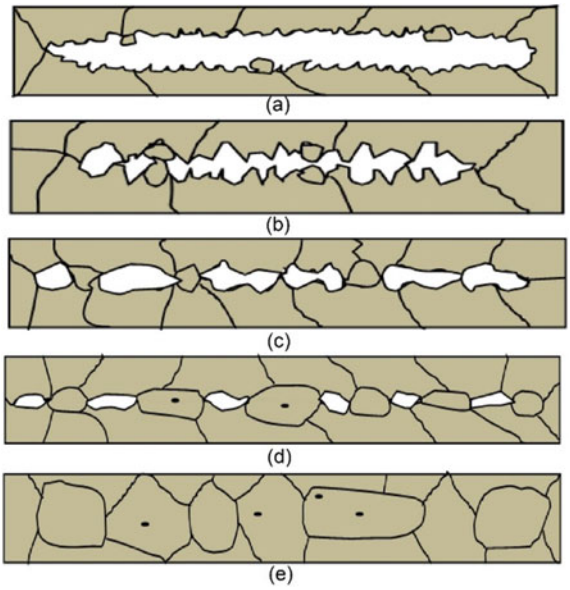

Fig. 2.16 Interface bonding mechanism of laminates subject hot roll bonding

Table 2.1 Illustration of roll bonded Cu/Al/Cu clad sheets

Sample (%)	Rolling reduction (%)	Condition
W-50	50	With SUS304 interlayer
W-70	70	With SUS304 interlayer
W-80	80	With SUS304 interlayer
WO-50	50	Without interlayer
WO-70	70	Without interlayer
WO-80	80	Without interlayer

by using rolling bonding. The peeling strength, morphologies of peeling surface, element diffusions and microstructure were examined, then the enhancement mechanism of SUS304 interlayer on the interfacial bonding strength of Cu/Al laminates was systematically discussed by combining the regulation of IMCs, mechanical joggle and shear deformation [11].

Figure 2.17 displays the peeling strength of Cu/Al/Cu laminates with or without SUS304 interlayer subjected to different rolling reduction. The peeling strength increased with the rolling reduction. When the rolling reduction was relatively low of 50%, both W-50% and WO-50% presented the same trend that peeling strength was almost parallel to the X-axis at value close to 0, which meant the dissimilar metals were not bonded well. When the rolling reduction increased to 70%, the peeling strength curves of W-70% and WO-70% became totally different. The peeling strength of WO-70% kept the origin trend and had a slight improvement to 2.9 N/mm, whereas, the peeling strength of W-70% presented a peak-valley shape. The